Stability of aerosol droplets in Bessel beam optical traps under constant and pulsed external forces

Journal Article

Author(s):
David, Grégory; Esat, Kivanç; Hartweg, Sebastian; Cremer, Johannes; Chasovskikh, Egor; Signorell, Ruth

Publication date:
2015-04-21

Permanent link:
https://doi.org/10.3929/ethz-b-000100895

Originally published in:
The Journal of Chemical Physics 142(15), https://doi.org/10.1063/1.4917202

Stability of aerosol droplets in Bessel beam optical traps under constant and pulsed external forces

Cite as: J. Chem. Phys. **142**, 154506 (2015); https://doi.org/10.1063/1.4917202
Submitted: 23 January 2015 . Accepted: 22 March 2015 . Published Online: 20 April 2015

Grégory David, Kıvanç Esat, Sebastian Hartweg, Johannes Cremer, Egor Chasovskikh, and Ruth Signorell

THE JOURNAL OF CHEMICAL PHYSICS 142, 154506 (2015)

Stability of aerosol droplets in Bessel beam optical traps under constant and pulsed external forces

Grégory David, Kıvanç Esat, Sebastian Hartweg, Johannes Cremer, Egor Chasovskikh, and Ruth Signorell[a)]
Laboratory of Physical Chemistry, ETH Zürich, Vladimir-Prelog-Weg 2, CH-8093 Zürich, Switzerland

(Received 23 January 2015; accepted 22 March 2015; published online 20 April 2015)

We report on the dynamics of aerosol droplets in optical traps under the influence of additional constant and pulsed external forces. Experimental results are compared with simulations of the three-dimensional droplet dynamics for two types of optical traps, the counter-propagating Bessel beam (CPBB) trap and the quadruple Bessel beam (QBB) trap. Under the influence of a constant gas flow (constant external force), the QBB trap is found to be more stable compared with the CPBB trap. By contrast, under pulsed laser excitation with laser pulse durations of nanoseconds (pulsed external force), the type of trap is of minor importance for the droplet stability. It typically needs pulsed laser forces that are several orders of magnitude higher than the optical forces to induce escape of the droplet from the trap. If the droplet strongly absorbs the pulsed laser light, these escape forces can be strongly reduced. The lower stability of absorbing droplets is a result of secondary thermal processes that cause droplet escape. © *2015 AIP Publishing LLC.* [http://dx.doi.org/10.1063/1.4917202]

I. INTRODUCTION

Single particle optical trapping allows for the investigation of aerosol particles under contact-free and well-controlled (temperature and relative humidity) conditions. Single particle studies are important to avoid ensemble averaging.[1] In contrast to ensemble measurements, they allow one to accurately quantify the particle size, which is crucial for size-dependent studies. Contact-free conditions are particularly important for studies on aerosol droplets or metastable states of aerosol particles, which play an important role in atmospheric processes. To characterize optically trapped particles or to control the conditions in their surroundings, additional external forces are often applied (see Refs. 2–12 and references therein). These can be constant forces or short-duration pulsed forces, such as, for example, a constant gas flow that is used to control the relative humidity of the particle's surroundings or a pulsed laser that is used for ablation studies or spectroscopic investigations of particles, respectively. External forces strongly influence the dynamics of the trapped particles. They typically reduce the particle stability in the trap hindering such investigation. This can be improved by using the proper type of optical trap, the choice of which, however, needs a detailed understanding of the dynamics.

In the present work, we study the dynamics of aerosol droplets in optical traps under the influence of additional constant and pulsed external forces with the goal to better understand the influence of the type of trap and external force. For this purpose, we combine experimental results with full three-dimensional simulations of the droplet dynamics.[13] Two types of optical traps that consist of multiple Bessel beams (BBs) are compared: the counter-propagating Bessel beam (CPBB) trap and the quadruple Bessel beam (QBB) trap. BB traps are versatile. For example, submicron-sized aerosol particles and multiple aerosol particles can be trapped or aerosol particles can be guided using BBs.[5,9,10,14] Furthermore, in BB traps, all optical components can be placed several centimeters away from the trapping region, which allows for an optimal control of the conditions (temperature) in the particle's surroundings.[15] This is more difficult using optical tweezers, which typically have working distance shorter than 1 mm.[12] Dual-beam optical tweezers have been reported that also can provide working distance of a few millimeters[16,17] or centimeters,[11] which is closer to the working distance of BB traps. It has not yet been investigated how BB traps and such dual-beam optical tweezers compare. Such a comparison is beyond the scope of the present paper. The CPBB trap consists of two counter-propagating BB arms (left panel in Fig. 1). It was first proposed by Cizmàr *et al.*[18] and later used for single aerosol particle studies (see Refs. 9, 19 and references therein). The QBB trap (middle panel in Fig. 1) is composed of two identical CPBB traps arranged perpendicularly to each other. It has been proposed by Thanopulos *et al.*[13] but not yet realized experimentally. Simulations reveal that aerosol particles in a QBB trap should be more stable and much better confined compared with a CPBB trap.[13] Furthermore, the QBB trap is less sensitive to imperfections in the optical alignment and its performance can be better predicted. In this paper, we use a constant gas flow to mimic the constant external force, which acts on the droplets from two different spatial directions as indicated in Fig. 1. These external forces are used to determine the stability and confinement of the droplets

a)Author to whom correspondence should be addressed. Electronic mail: rsignorell@ethz.ch

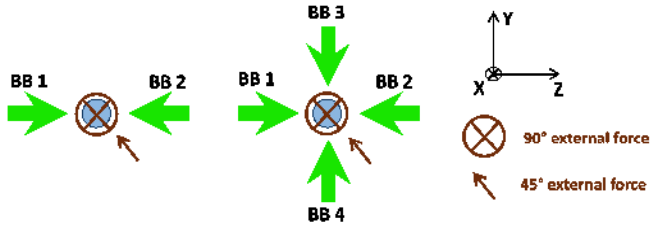

FIG. 1. Left: a CPBB trap consisting of two BB arms, BB1 and BB2. Middle: a QBB trap consisting of two CPBBs, CPBB1 and CPBB2. CPBB1 consists of BB1 and BB2 only and CPBB2 consists of BB3 and BB4 only. Right: axis system and symbols for the external forces. The blue circle symbolizes the trapped droplet. The green thick arrows indicate the individual BBs. The brown crossed circle stands for a constant external force that acts along the X direction (referred to as "90° external force"). The brown thin arrow indicates either a constant external force or a pulsed external force that acts in the YZ plane at an angle of 45° with respect to the BBs (referred to as "45° external force").

in QBB and CPBB traps. Short-duration (nanoseconds) laser pulses mimic the pulsed external force. These pulsed force experiments are performed for two types of droplets: droplets that do not absorb at the wavelength of the pulsed laser and droplets that strongly absorb at this wavelength. The QBB and CPBB experimental setups are explained in Sec. II. Section III presents the simulations of the three-dimensional droplet dynamics under constant and pulsed external forces. The results for the constant and pulsed external forces are presented in Secs. IV and V, respectively.

II. EXPERIMENTAL

A. BB setup, droplet generation, and sizing

Fig. 2 presents a scheme of the experimental setup. The beam radius of the Gaussian beam from the 532 nm continuous wave laser (Laser Quantum, Opus 3, typical power range used 500-1500 mW) is expanded from 0.8 mm to 1.6 mm by a telescope composed of two lenses with 50 mm and 100 mm focal lengths. The expanded beam is split into two orthogonally polarized laser beams of identical power using a half-wave plate ($\lambda/2$) and a polarization beam splitter cube (PBC). Two CPBB traps, CPBB1 consisting of BB1 and BB2 and CPBB2 consisting of BB3 and BB4 (Figs. 1 and 2), respectively, are formed from these two laser beams. For each CPBB, a BB is created from the incident Gaussian beams by an axicon with an apex angle of 178° and split into two orthogonally polarized BB arms of identical power using a $\lambda/2$ plate and a PBC. Typical powers per BB arm are in the range between 100 and 300 mW. Each of the two BB arms of a CPBB is then mapped to the centre of the trapping cell (trapping region) by a telescope composed of two lenses of 500 mm and 75 mm focal lengths, which results in BB core radii of 3.36 μm. The power in the core typically varies between 3 and 8 mW. For each CPBB trap, the corresponding two BB arms are aligned to be parallel and to have their cores overlapping in the centre of the trapping region to form a stable CPBB trap of several k_bT trap depths[13] (k_b is Boltzmann's constant and T = 293 K is the temperature). The latter requires the relative positions of the intensity maxima of two counter-propagating BB arms to be shifted along the direction of the laser propagation by distances dZ and dY for CPBB1 and CPBB2, respectively. These dZ and dY shifts do not influence the alignment of the core of the BB. As outlined in Ref. 13, the quality of the alignment is crucial because in particular small relative tilts (on the order of 1°) can strongly reduce the stability of a CPBB trap.

The QBB trap is simply composed of two perpendicularly arranged CPBB traps (CPBB 1 and CPBB 2). To form a stable QBB trap, the two CPBBs are aligned to be in the same plane

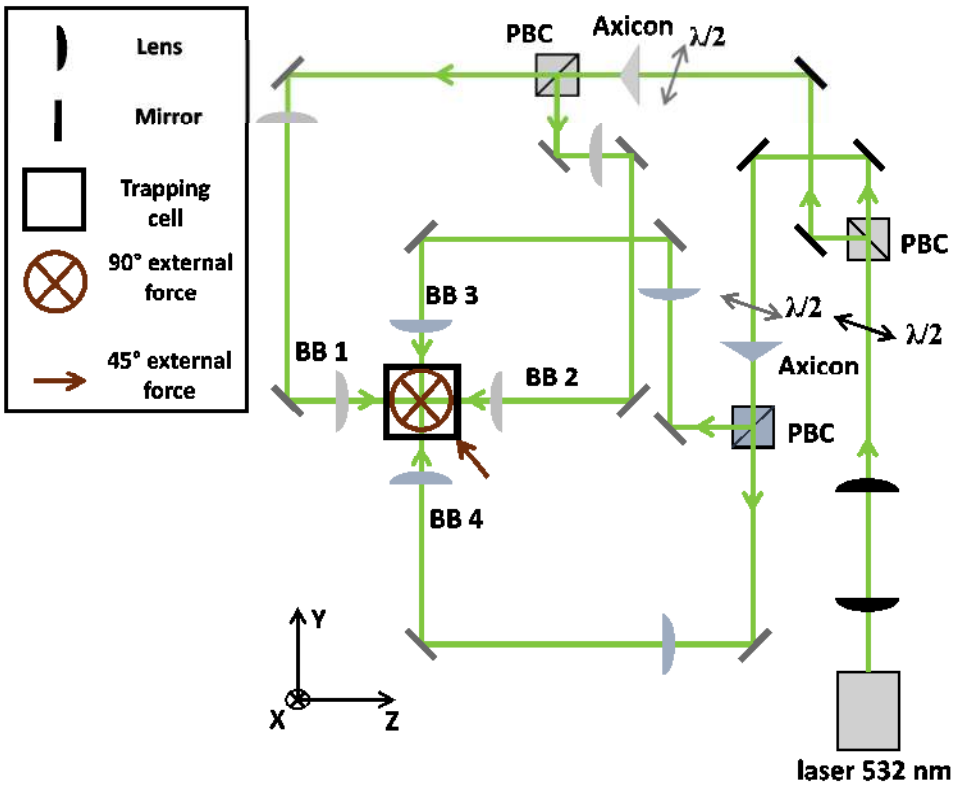

FIG. 2. Schematic of the optical layout with trapping cell and external forces. The optical setups used for droplet sizing ("angle resolved light scattering" and "broadband light scattering") are not shown in this scheme (see text).

(YZ) with all four BBs arranged perpendicular to each other so that the cores of the four BBs overlap in the centre of the trapping region. According to the simulations results from Ref. 13, the alignment of a QBB trap is much less critical for the stability compared to a CPBB trap.

Experiments are performed for saturated aqueous (H_2O, Merck Millipore, Lichrosolv®) NaCl (Merck Millipore, EMSURE®) droplets and for DOP (bis-(2-ethylhexyl)phthalate, Merck Millipore, purity >99%) droplets. A medical nebulizer (PARI LC SPRINT Nebulizer) and nitrogen gas (N_2; Pangas, nitrogen 5.0, ≥99.995%) are used for droplet generation. Single droplets are captured in the optical traps from a plume of dispersed aerosol generated by the nebulizer.

Two different light scattering methods are used to determine the radius of the droplets in the traps, which are referred to as "angle-resolved light scattering" and "broadband light scattering," respectively. As regards the size accuracy required for the present study, both methods provide equivalent results so that for a certain experiment we simply use the one that is more convenient in terms of space for optical components and simplicity of data processing. For the angle-resolved light scattering, the light from the trapping laser that is elastically scattered by the droplet is collected with an objective (Newport M-10X, working distance = 5.5 mm, NA = 0.25) as a function of the scattering angle θ over the range $75.5° < \theta < 104.5°$ and detected by a CMOS camera (Thorlabs, DCC1645C). The scattering phase function is retrieved from the camera images and the droplet radius r is determined by fitting the experimental phase functions to Mie theory. More details can be found in Refs. 9 and 20. Details of the broadband light scattering setup will be the subject of a forthcoming publication (see also Refs. 21–23). Briefly, the particle is illuminated by a focussed broadband light source (fibre coupled Xe lamp; Ocean Optics), which covers the wavelength range from about 250 to 2000 nm. The broadband light scattered by the particle around a scattering angle of $0 \sim 90°$ ($75.5° < 0 < 104.5°$) is collected and focused on a fibre which is coupled to a CCD spectrometer (Ocean Optics, Maya pro, 200-1100 nm). The droplet radius is determined by fitting the measured wavelength-dependent scattering cross section to the calculated wavelength-dependent scattering cross section using Mie theory.[20,21] The dispersion is assumed to be $m(\lambda) = m_0 + m_1/\lambda^2$ as suggested by the Cauchy equation (m is the real part of the index of refraction at wavelength λ, m_0 is the non-dispersive part, and m_1 is the dispersive part of m[24]). Fig. 3 shows an example for broadband light scattering. Overall, the agreement between experimental and fitted spectrum is good. The major deviation comes from differences in the wavelength-dependence of the baseline, which, however, does not influence the fitted radius. These deviations arise from the divergence and the chromaticity of the broadband light source and from optical aberrations. To minimize the chromaticity, we use reflective objectives and collimators.

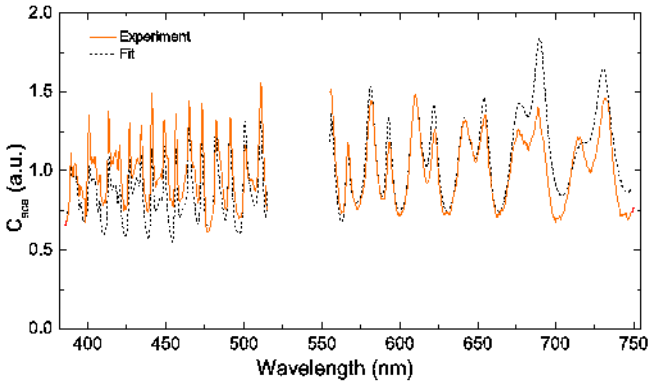

FIG. 3. Experimental broadband light scattering cross section (orange full line) and fitted broadband light scattering cross section (black dashed line) as a function of the wavelength for an aqueous NaCl droplet with a radius of $r = 1575$ nm.

B. External forces and escape forces

To compare the droplet stability in a CPBB versus a QBB trap, two different types of forces, a constant force and a pulsed force are exerted on the trapped particle. The constant force is realized by a continuous humidified N_2 gas flow that is either directed in the YZ plane at 45° with respect to the BBs (referred to as "45° external force") or along the X direction (referred to as "90° external force") as indicated in Figs. 1 and 2. These constant force experiments were performed on saturated aqueous NaCl droplet. The magnitude of the constant force can be varied and is controlled by a flow controller (Bronkhorst, F-201CV). To retrieve the constant force from the gas flow, we use Stokes law

$$F = 6\pi\eta r v, \tag{1}$$

where $\eta = 1.82 \cdot 10^{-5}$ Pa s is the viscosity of the surrounding gas, r is the particle radius, and v is the velocity of the gas at the droplet location. r is determined from the light scattering experiments (Sec. II A). The velocity v is derived from simulations performed with COMSOL Multiphysics.[25] For these simulations, the shape of the trapping cell and the geometry of the connecting tubing are modelled to reproduce the experimental setup as accurately as possible. The simulation starts with a N_2 gas flow equal to the experimental N_2 flow at the inlet of the nitrogen flow tubing which is propagated inside the tubing and the trapping cell. Simulations are performed for all different experimental N_2 flows and all different tubing geometries. (Note that for the 45° and 90° force experiments, different tubing geometries are used.) The velocity v is extracted from these simulations at the location of the droplet and the corresponding force is calculated from Eq. (1). These forces are used to characterize the stability of a trap (see "escape force" below).

A pulsed ultraviolet (UV) laser (Quantel, 266 nm wavelength, 7 ns pulse duration, and repetition rate <20 Hz) is used to apply a short-duration pulsed force to the droplets. The pulse repetition rate of ~0.5 Hz ensures that the single droplets reach a stable state after each pulse before being excited by a next pulse. These pulsed force experiments are performed for two types of droplets, for DOP droplets, which strongly absorb 266 nm light, and for aqueous NaCl droplets, which do not absorb 266 nm light. The UV laser beam is slightly focussed on the droplet with a lens of 1000 mm focal length, resulting in a 0.5 mm UV beam radius at the droplet location.

All pulsed experiments are performed with the laser beam in the YZ plane at 45° with respect to the BBs (45° external force in Figs. 1 and 2). The laser power can be varied by about a factor of ~10 between 0.45 and 3.3 mJ per pulse by changing the Q-switch time of the UV laser. The force F acting on the particle is determined from the experimental light intensity I from[20,26]

$$F = I(C_{ext} - C_{sca}\langle\cos\theta\rangle)/c, \tag{2}$$

where C_{ext} is the extinction cross section of the droplet, C_{sca} is the scattering cross section of the droplet, $\langle\cos\theta\rangle$ is the asymmetry parameter (average cosine of the scattering angle), and c is the velocity of light. I is calculated from the experimental laser pulse energy, from the laser pulse duration (7 ns full width half maximum (FWHM)), and the laser beam radius at the particle location (0.5 mm). It typically varies between $I = 0.13$ and 1.13 J s$^{-1}\mu$m^{-2}. C_{ext}, C_{sca}, and $\langle\cos\theta\rangle$ are calculated with a T-matrix code,[27] which enables one to accurately compute these properties for particle size parameters ($a = 2\pi r/\lambda$) up to $a = 70$. We use a refractive index of $m = 1.42 - 0{\cdot}i$ for the aqueous NaCl droplets[28] and a refractive index of $m = 1.486 - 0.01{\cdot}i$ for the DOP droplets. The imaginary part of the DOP refractive index was determined from spectroscopic measurements of DOP solutions at our analytical service facility and the real part of the refractive index is taken from Ref. 29.

To characterize the stability of a trap, we define an escape force F_{esc}. It corresponds to the external force at which the droplet either escapes from the trap or shifts by more than 100 μm from its initial trapping position. F_{esc} is determined from Eq. (1) for the constant force experiments and from Eq. (2) for the pulsed force experiments by gradually increasing the continuous gas flow or the laser power, respectively, and by determining the escape velocity v_{esc} and the escape intensity I_{esc}, respectively, at which the droplet escapes from the trap or shifts by more than 100 μm. Stability experiments are performed for droplets of different size and composition and for different powers of the BB arms, namely, for 100, 200, and 300 mW per BB arm (Sec. II A). A shift of more than 100 μm is considered to be equivalent to an escape from the trap because after such a pronounced shift the droplet can longer be observed or characterized by scattering or spectroscopy. Such shifts instead of proper escapes are sometimes observed for CPBB traps but not for QBB traps as further outlined in Sec. IV A (Fig. 4 (Multimedia view)). Experimentally, the particle escape and shift are measured with a microscope objective (Newport M-10x) and a CCD camera (Thorlabs DCC1645C). The size of the camera image is calibrated to quantify the particle shift. For that purpose, a trapped particle is first shifted from the centre of the camera image by applying a constant N_2 flow. Then, the translation stage (Newport 9063-XYZ) holding the objective and the camera is moved until the droplet is again in the centre of the camera image. The displacement of the droplet is then determined from the shift of the translation stage. This is done for different droplet displacements to calibrate the whole range of the camera image.

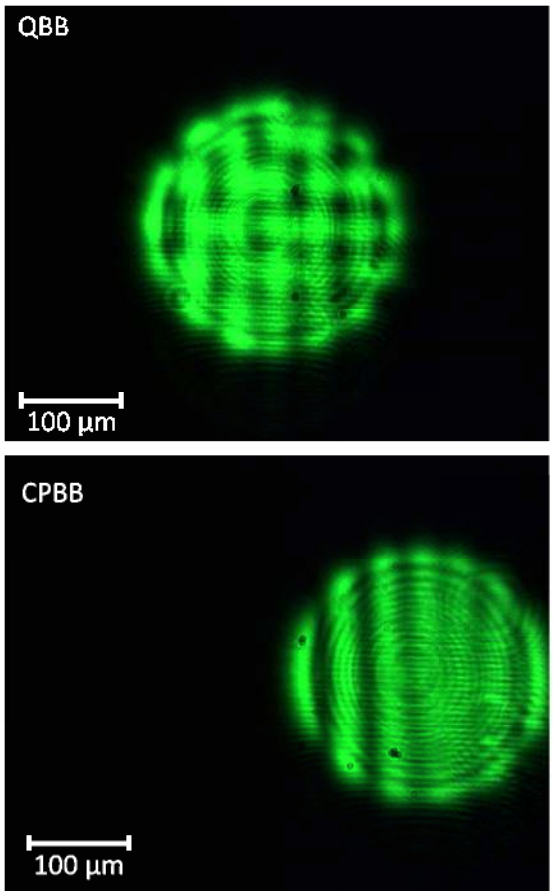

FIG. 4. Typical droplet dynamics in QBB (upper panel) and in CPBB (lower panel) traps under the influence of a constant 45° external force of increasing magnitude. Upper snapshot: droplet is in the centre of the QBB trap. Lower snapshot: droplet is shifted by 130 μm away from the centre of the CPBB trap. Same view as sketched in Fig. 1. The horizontal direction (Z direction) corresponds to the axial direction of the CPBB trap (CPBB1 in Fig. 1). (Multimedia view) [URL: http://dx.doi.org/10.1063/1.4917202.1] [URL: http://dx.doi.org/10.1063/1.4917202.2]

III. SIMULATION OF DROPLET DYNAMICS

To compare experimental results with simulations, we calculate the dynamics of droplets in the CPBB and QBB traps from the Langevin equation as described in Ref. 13 but in the presence of additional external forces $\boldsymbol{F}$ (Eqs. (1) and (2)),

$$\frac{d^2\mathbf{R}}{dt^2} = -\Gamma\frac{d\mathbf{R}}{dt} + \boldsymbol{F}_{opt}(\mathbf{R})/M + \boldsymbol{F}(t)/M + \zeta(t)\sqrt{2k_bT\Gamma/M}, \tag{3}$$

where $\mathbf{R}$ are the Cartesian coordinates of a droplet with respect to the (X, Y, Z) axis system indicated in Fig. 1 with the origin of the coordinate system in the centre of the trap. Γ is the damping constant of the surrounding gas (calculated from the viscosity given in Sec. II B), $\boldsymbol{F}_{opt}(\boldsymbol{R})$ is the total optical force that acts on the particle, M is the mass of the droplet, $\zeta(t)$ denotes Gaussian noise with zero mean and unit variance, k_b is Boltzmann's constant, and T is the temperature ($T = 293$ K). $\boldsymbol{F}_{opt}(\boldsymbol{R})$ is calculated by integrating Maxwell's stress tensor over a closed surfaced containing the trapped particle. For details, see Ref. 13. We assume that $\boldsymbol{F}_{opt}(\boldsymbol{R})$ is the incoherent sum of the optical forces arising from the individual BB arms. This is consistent with the experimental setup in Fig. 2, for

which the lengths of the different BB arms are different to avoid interference. The simulated BBs have the same properties as the experimental ones, namely, a wavelength of 532 nm, a core radius of 3.36 μm, a diffraction-free propagation distance of Z_{max} = 4.1 mm, powers of 100, 200, or 300 mW per BB arm, and the same polarization as the experimental beams (Fig. 2). The refractive indices of droplets are given in Sec. II B. Optical forces are calculated for perfectly aligned and for tilted CPBB and QBB traps with 1° relative tilt between the two BBs (see Ref. 13 for details). Other imperfections in the alignment of the BBs, such as the relative slips between BB arms, are not taken into account here because they have been shown to be much less important for the trapping stability.[13]

The $F(t)$ for the 45° and 90° external force simulations are described in Sec. II B. For the pulsed force, either a 7 ns boxcar force or a 7 ns FWHM Gaussian force is modelled in agreement with the 7 ns FWHM duration of the UV laser pulse in the experiment. Essentially, identical results are obtained for the boxcar and the Gaussian pulse shape. The repetition rate of the simulated pulses equals 2 Hz to allow the droplet to return to a steady state before being excited again by a new force pulse in agreement with the experiment.

The Langevin equation is solved using a Verlet algorithm.[30] A minimum time step of 100 ns is used. This time step is decreased to 0.1 ns during 1 μs following the beginning of the pulsed force to ensure numerical smooth change of the force. The position of the particle is recorded every 10 ms for the constant force simulations and every 100 μs for the pulsed force simulations to obtain a trajectory. The trajectory ends at a preset maximum time or with the escape of the droplet, whichever comes first. Maximum simulation times are on the order of many hundred seconds. To determine the escape force F_{esc}, the following criteria were used. In the CPBB trap, the particle is considered to have escaped from the trap if it is shifted by more than 4.5 μm from the centre of the trap in lateral direction (XY plane for CPBB1 in Fig. 1) or if it is shifted by more than 100 μm along the axial direction (Z direction for CPBB1). 4.5 μm is more than the lateral trap dimension of a CPBB. In the QBB trap, the particle is considered to have escaped from the trap if it shifts by more than 4.5 μm from the centre of the trap in X, Y, or Z direction, i.e., by more than the trap dimension. Note that droplets in CPBB traps are much less confined along the axial direction (typical confinement on the order of 2.5 μm for a 1.4 μm particle without external forces) compared with QBB traps (typical confinement on the order of 30 nm for a 1.4 μm particle without external forces).

IV. CONSTANT EXTERNAL FORCES

A. Experimental results

Fig. 4 (Multimedia view) shows typical droplet dynamics observed in QBB (upper panel) and in CPBB (lower panel) traps under the influence of an external force of increasing magnitude. At the beginning, no external force is applied. The particle in the QBB trap without external force is well-confined in the centre of the trap. With increasing external force, the droplet remains stable in the centre of the QBB trap until the particle suddenly escapes from the trap when the external force equals the escape force. The dynamics in the QBB trap is reproducible and not very sensitive to the particular trap alignment. This is due to the strong gradient forces that act in all directions in a QBB trap and is consistent with the modelling prediction from Ref. 13. The dynamics in the CPBB trap is different. Even with no external force applied, the droplet in the CPBB trap may wobble by tens of micrometers in axial direction (direction of laser propagation) around its stable position as a consequence of the weak confinement of a CPBB trap in axial direction. As soon as the external force is turned on, the droplet immediately shifts in axial direction where the optical force originates from a fragile balance of scattering forces. The displacement of the droplet increases gradually with increasing external force. This displacement seems to be linear with the increase of the flow and hence the external force. In some experiments, the droplet stops shifting with increasing external force and then suddenly escapes from the trap (not shown in the video) for displacements of the droplet from the trap centre of less than 100 μm. In these cases, the escape force F_{esc} is determined from the external force applied at the moment of escape (Eq. (1)). In other experiments, as the one shown in the lower panel in Fig. 4 (Multimedia view), the droplet is shifted by more than 100 μm away from the trap centre without escaping. Here, we use the external force needed to induce a shift of 100 μm to determine F_{esc}. In contrast to QBB traps, the droplet dynamics in CPBB traps is not very reproducible and depends strongly on the trap alignment in agreement with the modelling prediction from Ref. 13. This is mainly a consequence of the fragile balance of scattering forces that act in axial direction. Strong retaining gradient forces only act laterally in a CPBB trap. The droplet dynamics for the 45° external force and the 90° external force is qualitatively similar. In both cases, the droplet shifts along the Z-axis when the force is applied. For the 90° force, this can be explained as follows: the 90° force in X-direction moves the droplet slightly away from the exact center of the trap so that the scattering forces from the BBs are no longer equal due to polarization effect. Hence as only the balance of these scattering force confines the droplet along the Z-axis in the CPBB trap, the droplet is shifted along Z-axis as soon as the force is applied. However, for the same external force, the absolute displacements of the droplets are smaller for the 90° case compared with the 45° case and it needs higher values for the 90° external force to remove the droplet from the trap.

The experimentally observed droplet dynamics is quantified in Fig. 5. It provides the normalized experimental escape forces F_{esc} for the 45° external force (upper panel) and the 90° external force (lower panel) as a function of the droplet radius. F_{esc} in Fig. 5 is normalized to a laser power per BB arm of 200 mW. Individual experiments are performed with different laser powers per BB arm of 100, 200, or 300 mW. As expected, F_{esc} is found to be proportional to the laser power per BB arm so that normalization of the data is appropriate (data not shown). As explained in Sec. II B, F_{esc} is retrieved from Eq. (1) by simulating the N_2 gas velocity at the particle location during its escape. The calculated N_2 gas velocities during the particle escapes vary between 0.26 and 9.3 mm s^{-1} (for flow rates at the tubing entrance of 0.8 and 19.3 standard cubic

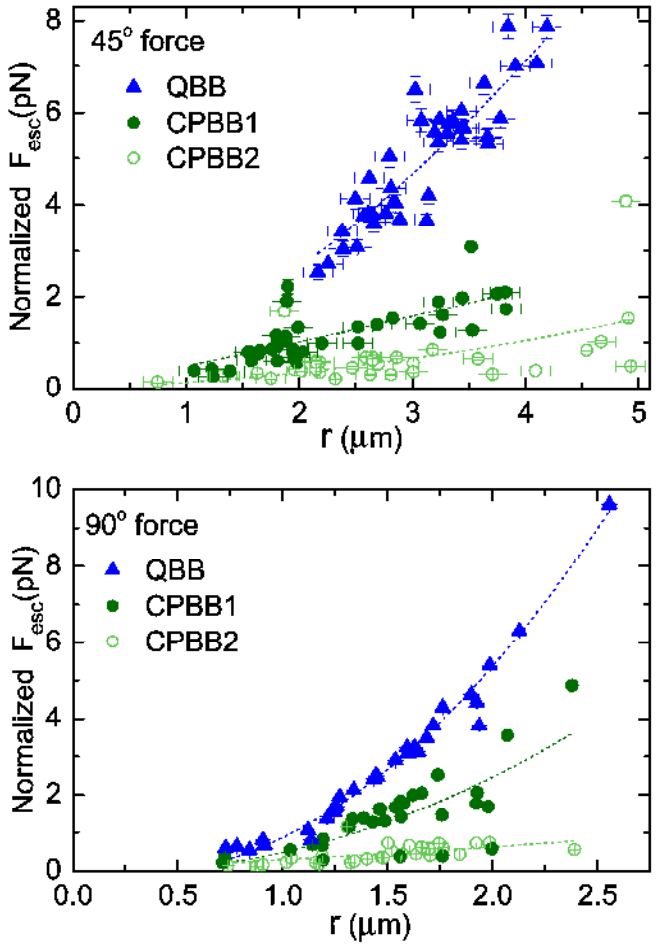

FIG. 5. Experimental escape forces F_{esc} normalized to a laser power of 200 mW per BB arm as a function of the droplet radius r for a constant 45° external force (upper panel) and a constant 90° external force (lower panel) measured for a QBB trap and two CPBB traps (CPBB1 and CPBB2). The dashed lines are to guide the eye and have no other meaning. Note that the force and the radius scale are different in the two panels. The error bars are within the size of the symbols in the lower panel as broadband light scattering is used to size the particle.

centimeters, respectively) depending on the trap and particle size. At a certain flow rate, the COMSOL simulations show that the N_2 gas velocity changes by less than 1% in the volume over which the droplet moves during the experiment. Fig. 5 summarizes the data for F_{esc} for the QBB and the two CPBB traps CPBB1and CPBB2 (Fig. 1). The plotted error bars are determined from the uncertainty in the determination of the particle radius. The latter is around 130 nm when the scattering phase function is used to size the particle[9] (upper panel) and around 2 nm when broadband light scattering is used to size the particle[23] (lower panel). A first prominent trend in Fig. 5 is the increase in the trapping stability (F_{esc}) with increasing droplets size for all three traps. Furthermore, a comparison of the upper and the lower panel in Fig. 5 shows that for the same trap and the same droplet radius, the normalized F_{esc} is indeed higher for the 90° external force compared with the 45° external force, consistent with the qualitative observations described above. The third obvious trend in Fig. 5 is the higher stability of the QBB trap compared with an averaged CPBB trap. The normalized F_{esc} of the QBB is larger than the average of the normalized F_{esc} of CPBB1 and CPBB2. The comparison of CPBB1 and CPBB2 in Fig. 5 also illustrates that CPBB traps that should be identical according to the experimental layout can in reality behave quite differently. As discussed in Thanopulos *et al.*,[13] this is most likely a consequence of the sensitivity of the CPBB traps to small imperfections in the alignment, which can neither be avoided nor accurately specified in the experiment.

B. Simulation results

Typical results of the droplet dynamics obtained from simulations (Sec. III) are displayed in Figs. 6 and 7. The two examples summarize data for 45° and 90° constant external forces, two droplet sizes (1.4 μm and 2.8 μm), a perfectly aligned QBB (referred to as "perfect QBB"), a perfectly aligned CPBB (referred to as "perfect CPBB"), and for a QBB and a CPBB with minor relative tilts of 1° between the BBs (referred to as "tilted QBB" and "tilted CPBB," respectively). The droplet dynamics is visualized for the 45° external force by the average Y and average Z positions of the droplet and for the 90° external force by the average X and average Z positions, and by their respective standard deviations (STDs). The average droplet positions and the corresponding STDs are calculated along the whole simulated trajectory. An average position of zero means that the droplet has escaped before the first sampling point (i.e., within 10 ms). The axis system refers to Fig. 1 and the axial direction of the CPBB is chosen along Z.

In both the perfect and the tilted QBB traps, shifts in the average Y position of ~1.5 μm result in the immediate escape of the droplet from the trap. In the upper left panel of Fig. 6, for example, such an immediate escape is indicated at ~3600 fN by the sudden drop of the average Y position to zero as the droplet escapes from the trap within less than 10 ms. In the lower left panel of Fig. 6 and in the two left panels in Fig. 7, the droplets need more than 10 ms to fully escape from the trap. Here, the droplet moves along a more or less straight line towards the edge of the trapping region, with a correspondingly increased STD of the position. In the lower left panel of Fig. 6, e.g., this happens at ~11 500 fN. For the QBB traps, the behaviour in Z direction is very similar to that in Y direction; i.e., shifts of ~1.5 μm cause the immediate escape from the trap. Note that the details of the dynamics in Z directions are not visible in the right panels of Figs. 6 and 7 because of the different scales of the average Z position (several 10 to several 100 μm). The droplet dynamics of the perfect and the tilted QBB traps is almost identical, not only qualitatively but also quantitatively. Differences occur between the different force directions (45° in Fig. 6 and 90° in Fig. 7). At 90°, larger escape forces are needed than at 45°—otherwise the QBB shows the same qualitative behaviour for the two different force directions.

The dynamics in the CPBB traps is more versatile compared with the QBB traps. As described, the latter shows only immediate escapes. In a perfect CPBB trap and under a 45° external force (Fig. 6), the droplet first experiences an increasing shift in Z direction with increasing force but keeps a well-defined Z position (small STDs). At an even higher force,

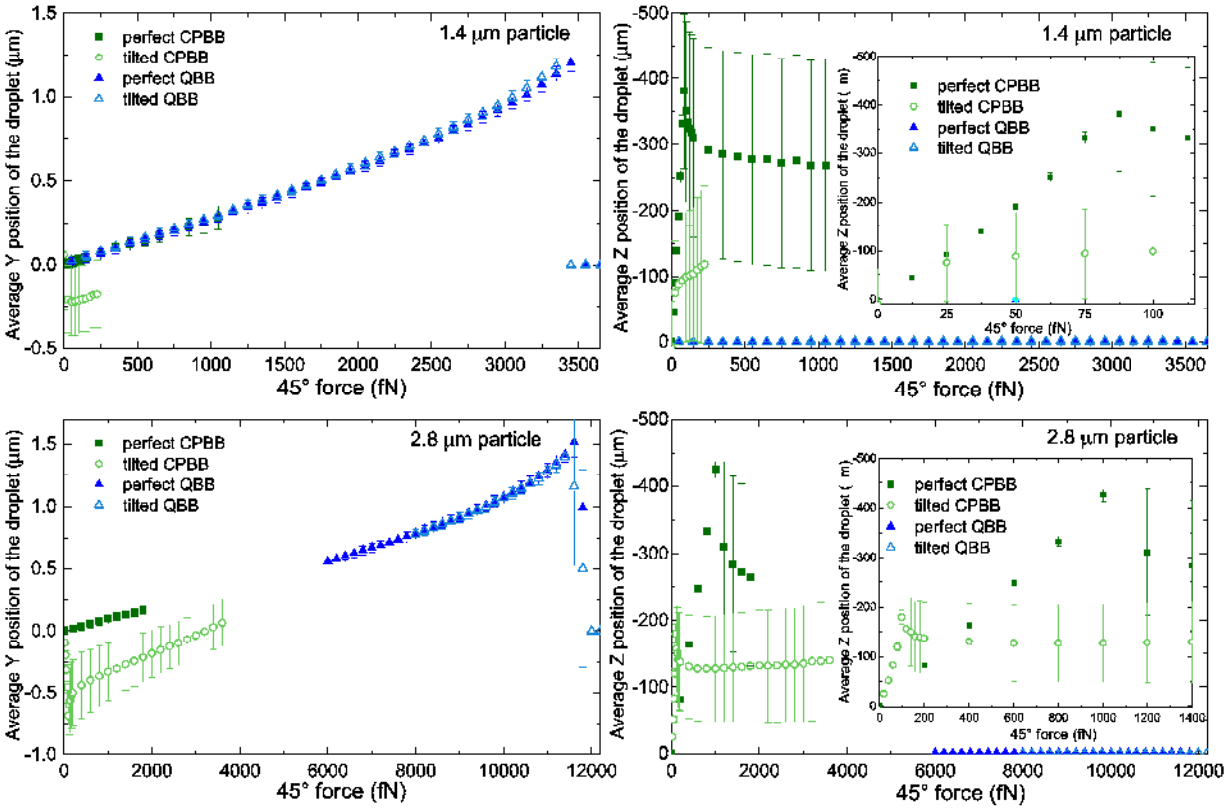

FIG. 6. Summary of the droplet dynamics obtained from simulations (Sec. III). The average droplet positions are shows as a function of a 45° constant external force. The error bars correspond to the standard deviations in the respective positions. The simulations are for traps with $dZ = 50\ \mu m$ (see Table I).

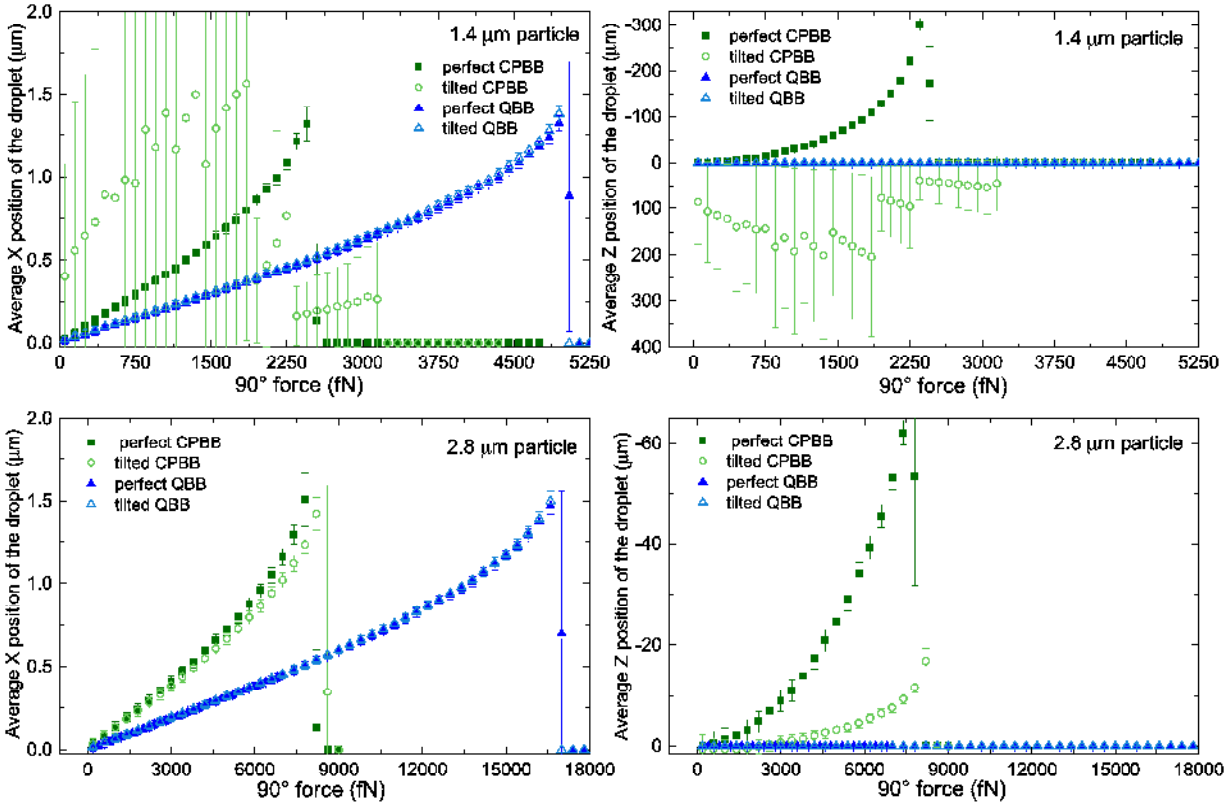

FIG. 7. The same as in Fig. 6 but for a 90° constant external force.

the droplet does no longer reach a well-defined Z position before it escapes, which is indicated by the strong increase in the STD for theses forces. As explained above, a strong increase in the STD indicates the onset of the escape from the trap. For the 1.4 μm droplet, this happens at an external force of ~80 fN and a shift in position relative to the trap centre of ~−370μm. The corresponding values for the 2.8 μm droplet lie between 1000-1200 fN and ~−400μm, respectively. The corresponding Y positions (left panels in Fig. 6) change only slightly. In summary, for the 45° force, we observe instead of immediate escapes as in the QBB traps first very pronounced Z shifts (much more than our cutoff criterion of 100 μm for F_{esc}, Sec. II B) before the particles completely escape. For the 90° force and perfect CPBB traps (Fig. 7), the type of dynamics is again similar to the ones found in the QBB traps; i.e., immediate escapes in X direction are observed at shifts in the X position of ~1.5 μm. For the 1.4 μm droplet, this happens at an external force of ~2500 fN and for the 2.8 μm at ~8000 fN. The major qualitative difference compared with the QBB traps is the fact that at the same time, also an appreciable shift in Z direction is observed with increasing external force. For the 2.8 μm droplet and for both the 45° and the 90° cases, the dynamics in the tilted CPBB traps is qualitatively similar to the ones observed in the perfect CPBB traps. The only difference is that the tilted traps tend to be less stable. The 1.4 μm droplet in the tilted CPBB traps is a special case. This droplet is not stable, not even at zero external force (see also Table I), which is indicated in the two upper traces of Figs. 6 and 7 by the huge STDs in the droplet positions and the large shifts away from the trap centre (X = Y = Z = 0) for all external forces.

Table I lists the normalized escape forces obtained from the different simulations as defined in Sec. III. The following three trends can be extracted from this table. The stability (F_{esc}) increases with increasing droplet radius for all different types of traps. The stability is higher for the 90° external force compared with the 45° external force for the same droplet size and the same trap type. And finally, the QBB trap is clearly more stable than the CPBB trap. (Note that only data for one CPBB trap are listed because CPBB1 and CPBB2 are identical in the simulations in contrast to the experiment.) The data in Table I also demonstrate that the QBB trap is much more robust against small misalignment of the BBs compared with the CPBB trap. The extreme case is the 1.4 μm particle, which in the tilted CPBB trap is not even stable in the absence of external forces so that $F_{esc} = 0$ (see Figs. 6 and 7).

C. Comparison experiment and simulation

The comparison of Fig. 5 and Table I reveals that the same qualitative trends are observed in the experiment and the simulations. The first trend, the increase in stability with increasing droplet radius, is common to all different types of traps. Qualitatively, this is an effect of the increase of the optical forces with increasing polarizability which roughly scales with the droplet volume. However, the quantitative agreement between experiment and simulation is rather poor, which is likely a consequence of imperfections in the alignment of the optical components in the experimental setup. That small imperfections can have a strong influence on the stability are demonstrated by the 1° tilt simulations in Table I. We would like to note here that the specific experimental imperfections in the alignment are unknown and thus cannot be modelled accurately, so that we can only demonstrate their principle influence.

The second trend, the higher stability for the 90° external force compared with the 45° external force, is also found in both experiment and simulation. For the CPBB traps, this trend is expected because the 90° external force acts mainly in X direction (Fig. 1), where strong gradient forces can stabilize the droplet to some extent. The 45° external force, by contrast, has one component that points into the direction (Z and Y directions for CPBB1 and CPBB2, respectively) where the fragile balance of scattering forces determines the stability. For the QBB, the higher stability under the influence of the 90° force might not be so obvious at first sight because gradient forces act here in all direction. It has, however, a simple explanation. The gradient force in X direction (Fig. 1) is approximately two times stronger than the gradient forces that act in the Y or the Z direction because the force in X direction is the sum of the gradient forces of CPBB1 and

TABLE I. Normalized simulated escape forces F_{esc} for constant 45° and 90° external forces calculate for two different droplet radii r in a QBB trap and a CPBB trap. Results are provided for perfect traps (tilt = 0°), for imperfect traps with tilted BBs (tilt = 1°), and for traps with two different relative distances dZ of the intensity maxima of counter-propagation BB arms.

				F_{esc} (pN)	
External force	r (μm)	Tilt in deg	dZ (μm)	QBB	CPBB
45°	1.4	0	50	3.55	0.0275
45°	1.4	1	50	3.45	0
45°	2.8	0	50	11.8	0.24
45°	2.8	1	50	11.6	0.07
45°	2.8	0	100	11.8	0.26
45°	2.8	1	100	11.6	0.09
90°	1.4	0	50	5.05	1.8
90°	1.4	1	50	5.05	0
90°	2.8	0	50	17.0	8.2
90°	2.8	1	50	17.0	8.6

CPBB2. Despite the QBB being approximately two times stronger than the CPBB1, again, no real quantitative agreement between experiment and simulation is found. In particular, the dramatic increase in stability for the CPBB trap predicted by the simulations is not reproduced by the experiment.

The higher stability of the QBB trap compared with the CPBB trap is the most important trend that is clearly visible in both experiment and simulation, albeit to different degrees. For the 2.8 μm droplet, the simulations predict 45° escape forces of 11.8 pN and 0.24 pN for perfect QBB and CPBB traps, respectively (Table I). This contrasts with corresponding experimental values of approximately (4.25 ± 0.20) pN and (1.02 ± 0.05) pN (averages of CPBB1 and CPBB2). For the 1.4 μm droplet, the predicted 90° escape forces of 5.05 pN and 1.8 pN for perfect QBB and CPBB traps, respectively, compare with experimental values of (2.25 ± 0.01) pN and (0.75 ± 0.01) pN (averages of CPBB1 and CPBB2). Compared with the experiment, the simulation overestimates the gain in stability of QBB vs. CPBB trap for the larger droplet, while for the smaller droplet, the relative increase in stability is comparable. The lower stability of the CPBB trap simply arises from the absence of strong gradient forces in axial direction. By contrast, in the QBB trap, strong gradient forces act in all direction.

V. PULSED EXTERNAL FORCES

External forces of short duration (nanoseconds or less) can, in principle, have a different influence on the dynamics of droplets in optical traps compared with constant external forces. Because of their short duration, the spatial displacement of the droplet away from the trapping position during the time the force is applied (referred to as "force pulse") is very small (less than nm) compared with the trap dimension. It is therefore not unreasonable that the droplet does not escape from the trap during the pulse and relaxes quickly after the force pulse is over. To test this hypothesis, we perform experiments with a 7 ns FWHM pulsed UV laser (266 nm) as external pulsed force and two different types of droplets, aqueous NaCl droplets and DOP droplets (Sec. II A). Aqueous NaCl droplets do not absorb 266 nm light ($m = 1.42 - 0 \cdot i$) while DOP droplets strongly absorb at this wavelength ($m = 1.486 - 0.01 \cdot i$). For the aqueous NaCl droplets and for light intensities of up to 1.13 J s$^{-1}\mu$m^{-2} (corresponds to 3.3 mJ per pulse for a 7 ns FWHM Gaussian pulse with a 0.5 mm radius), we observe no escape of the particles from the traps even though these pulsed laser forces are several orders of magnitude higher than the trapping forces (tens of nN versus pN). Note that a light intensity of 1.13 J s$^{-1}\mu$m^{-2} corresponds to an external pulsed force of $F \sim 35$ nN for a 2.8 μm radius droplet (Eq. (2)). The laser pulse has also no other observable effect on the non-absorbing droplets. These experimental results are in agreement with simulations of aqueous NaCl droplets (Sec. III), which confirm that the droplets should not escape from the trap under the influence of these pulsed forces (data not shown). The simulations predict that much higher external forces (more than several ten times higher) would be needed for the droplets to escape from the trap.

Unexpectedly, the experimental observations for the absorbing DOP droplets are completely different. These droplets already escaped from the traps at average light intensities of only $I_{esc} \sim 0.4$ J s$^{-1}\mu$m^{-2} for both the QBB and the CPBB traps. This average light intensity is determined from individual experiments with ~60 droplets (30 for the QBB and 30 for the CPBB) with radii between 1.7 and 2.4 μm. It corresponds to an average escape force of $F_{esc} \sim 31$ nN for a 2.8 μm particle. Escape from the traps is not the only observable effect after pulsed laser excitation of DOP droplets. Partial ablation/evaporation of the droplets caused by the laser is another phenomenon that is visible after laser excitation. This is illustrated in Fig. 8, which shows the scattered light from the droplet and a plume of ablated/evaporated material just above the scattered light of the droplet. This plume forms immediately after the laser pulse and disappears quickly after the pulse is over. In addition, the pattern of the scattered light is different before and after the pulse (not shown), which would be consistent with a change in droplet size caused by ablation/evaporation. The quantification of this size change was not possible within the precision of our phase function measurement.

To elucidate this behaviour, we have performed simulations of the droplet dynamics. Fig. 9 summarizes the corresponding results for a 1.4 μm (upper panel) and a 2.8 μm (lower panel) DOP particles after pulsed laser excitation for perfect and imperfect QBB and CPBB traps (Sec. III). The escape probability of a droplet per laser pulse is shown as a function of the external force (lower abscissa) and the laser intensity (upper abscissa) for a pulsed force with boxcar shape. It is defined as the ratio of the number of droplets that escape and the number of laser pulses. In the following, $F_{0.5}$ and the intensity $I_{0.5}$ correspond to the force and intensity, respectively, for which the escape probability has a value of 0.5. Fig. 9 shows that larger droplets are more stable (larger $F_{0.5}$) than smaller droplets. This is an effect of the higher mass of the particle, which for the same force moves less.

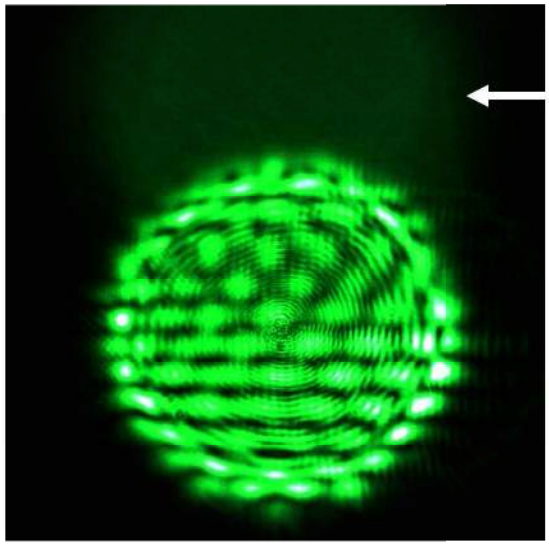

FIG. 8. Snapshot of a DOP particle in a QBB trap just after excitation by a 266 nm laser pulse. The bright irregular pattern is the light of the trapping laser that is scattered by the droplet. The faint shadow above the droplet (indicated by white arrow) corresponds to a plume of ablated/evaporated material after laser excitation.

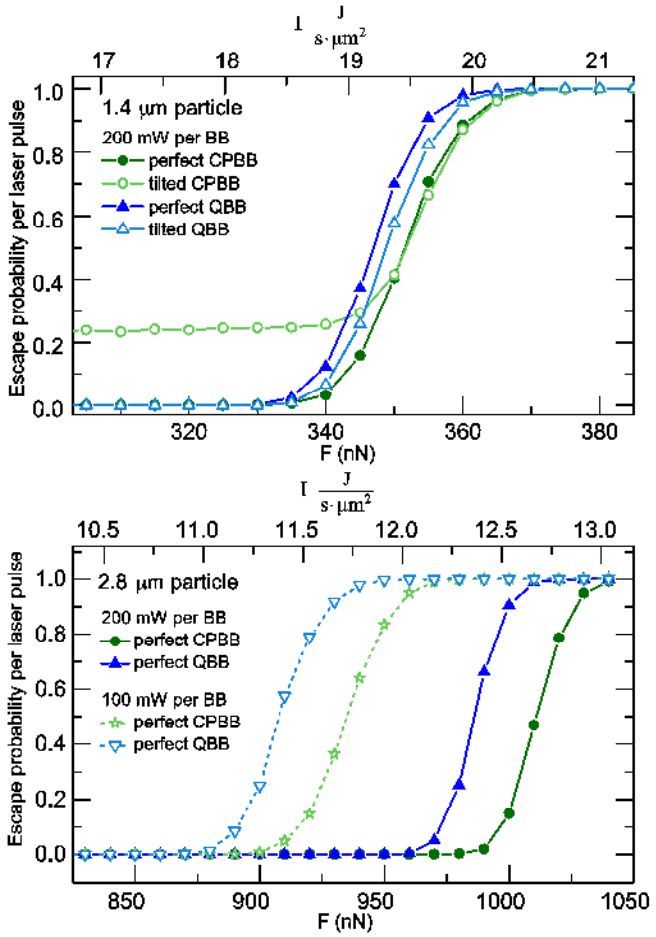

FIG. 9. Escape probability per laser pulse for a 1.4 μm (upper panel) and a 2.8 μm (lower panel) droplet as a function of the external pulsed force F (lower abscissa) and the laser intensity I (upper abscissa) for a pulsed laser force with boxcar shape of 7 ns duration and 266 nm wavelength. Most data are given for perfect and imperfect QBB and CPBB traps with 200 mW power per BB arm. The lower panel also contains data for 100 mW per BB arm.

Note that F_{esc} is higher for the large droplet although I_{esc} is lower for the large droplet (see data for 200 mW per BB) because the absorption and scattering cross section are larger for the larger droplet. All probability curves exhibit a very similar general behaviour. For small forces, the droplets cannot escape because their displacement away from the centre of the trap caused by the pulse is only minor. (Note that an escape probability larger than zero at low forces for the 1.4 μm particle in the tilted CPBB trap arises because this droplet is not stable in the trap even at zero external force.) As for the NaCl droplets, this demonstrates that pulsed laser forces that are several orders of magnitude higher than the trapping forces do not necessarily lead to droplet escape. For somewhat higher forces, the escape probability suddenly increases from 0 to 1 over an increase of the pulsed force of less than 5% (Fig. 9). At this point, the pulsed force is suddenly high enough to induce droplet displacements (on the order of the trap dimension) that result in direct escape. Fig. 9 also reveals that the type of trap has a comparatively weak influence on the absolute values of the probability curves and thus on $F_{0.5}$. This is because the pulsed forces are anyway much higher than the trapping forces and thus dominate the dynamics. The slightly but systematically higher stability of the CPBB traps compared with the QBB traps that is found in the simulations has the following reason: the axial dimension of the CPBB trap is much larger (~100μm) than that of the QBB trap (a few μm). To escape, the droplet must travel a longer distance in the CPBB trap, during which its motion is damped by the surrounding gas. As a consequence, the droplet is slightly more stable in the CPBB trap. The dominance of the pulsed force over the trapping forces is also exemplified by the minor difference between the simulations for 100 mW per BB arm and 200 mW per BB arm in the lower panel in Fig. 9. A decrease in the power of the trapping beam of a factor of 2 results in a decrease in $F_{0.5}$ of only ~10%.

In contrast to the NaCl droplet case, the simulation and the experimental results for DOP droplets do not agree with each other. In the experiment, the droplets escaped from the traps at escape intensities of $I_{esc} \sim 0.4$ J s^{-1} μm^{-2}. The simulation predicts that it needs at least an $I_{0.5}$ of 11 J s^{-1} μm^{-2}, which is 30 times higher than observed. This discrepancy together with the results for the NaCl droplets implies that it cannot be the optical force exerted by the pulsed laser on the DOP droplets that causes the escape of the droplets. We believe that secondary processes induced by the absorbed light are actually driving the droplet out of the traps. In contrast to light scattering, light absorption can induce different secondary thermal effects. They can range from photophoretic forces[31,32] to evaporation or ablation of the droplets. The light absorption may lead to non-uniform heating of the particle. The resulting temperature inhomogeneity creates a photophoretic force, which can be much higher than the photon pressure and hence could explain the observed effects.[31] In addition, as mentioned above, signs of strong ablation/evaporation are indeed observed for DOP droplets (Fig. 8). Such secondary thermal processes can cause "uncontrolled" momentum transfer from the ablated/evaporated matter to the remaining particle and thus result in droplet escape. Indications for ablation/evaporation are not observed for NaCl droplets consistent with the fact that they do not absorb 266 nm light. This prevents the escape of the NaCl droplets under our experimental conditions in agreement with the simulations.

VI. SUMMARY AND CONCLUSIONS

We compare the dynamics and in particular the stability of aerosol droplets in counter-propagating and in quadruple Bessel beam optical traps when these droplets are under the influence of an additional external force. The latter is simulated by a constant gas flow or a short-duration pulsed laser, respectively, i.e., by two types of forces that are relevant to single aerosol droplet studies. Experimental results are compared with simulations, which calculate the full three-dimensional droplet dynamics and which also take into account the influence of imperfections in the alignment of optical traps. We also present the first experimental realization and characterization of a QBB trap.

For a constant external force, the escape force (lowest external force that is needed to cause droplet escape from the trap) is on the same order of magnitude as the trapping forces (typically pN). The stability of a droplet thus sensitively

depends on the details of the optical trap used. Droplets in a QBB trap are found to be more stable under the influence of a constant external force than droplets in a CPBB trap. Escape forces in the QBB trap are up to several ten times higher than in a CPBB trap for droplets with radii between 1 and 3 μm. The reduced stability of the CPBB trap mainly arises from the difficulties in balancing the scattering forces in axial trap direction. The QBB trap does not have this deficiency because strong gradient forces act here in all directions. This is also the reason why the droplet confinement is much better in the QBB trap. Both experiments and simulations show a multifaceted droplet dynamics. In the QBB trap, the droplets immediately escape from the trap when the external force reaches the escape force. The displacement of the droplet from the trap centre at the point of escape is on the order of the BB core size (less than a few μm). In the CPBB traps, the droplets always shift by several ten to several hundred μm in axial direction before they finally escape. The QBB trap is much more suitable to perform constant force experiment on single droplets because of the higher stability, the better confinement, and the lower sensitiveness to imperfections in the optical alignment.

For the pulsed external force, the type of trap has only a minor influence on the droplet stability for laser pulses of several ten nanoseconds duration. The pulsed escape forces are several orders of magnitude higher than the trapping forces (tens of nN versus pN). The escape forces are so much higher than the trapping forces because the droplet only escapes if it can do so more or less ballistically, i.e., before the damping by the surrounding medium can relax and restabilize it. We further find non-absorbing droplets to be significantly more stable compared with strongly absorbing droplets. The comparison of experiments and simulations indicates that secondary thermal processes such as photophoresis, droplet evaporation, or ablation are responsible for the reduced stability of absorbing droplets.

In summary, the QBB trap is more suitable for experiments with external forces even for pulsed external force where no pronounced difference in stability between QBB and CPBB traps exists. Its performance is more predictable, it is less sensitive to imperfections in the optical alignment, and the confinement of the droplets is much better. The latter is particularly important for droplet characterization, e.g., by light scattering where the quality of the scattering pattern hinges on tight droplet confinement.

ACKNOWLEDGMENTS

We are very grateful to David Stapfer and Markus Steger from the LPC shops for their assistance in developing the experimental setup, to Dr. David Luckhaus for his advice concerning the calculations, and to Guido Grassi for the DOP refractive index measurements. Financial support was provided by the ETH Zürich and the Swiss National Science Foundation (SNF Project No. 200021_146368).

[1]M. Nirmal, B. O. Dabbousi, M. G. Bawendi, J. J. Macklin, J. K. Trautman, T. D. Harris, and L. E. Brus, Nature **383**, 802 804 (1996).
[2]L. Malmqvist and H. M. Hertz, Appl. Opt. **34**, 3392-3397 (1995).
[3]K. C. Neuman and S. M. Block, Rev. Sci. Instrum. **75**, 2787-2809 (2004).
[4]F. L. Mao, Q. R. Xing, K. Wang, L. Y. Lang, Z. Wang, L. Chai, and Q. Y. Wang, Opt. Commun. **256**, 358 363 (2005).
[5]M. D. Summers, J. P. Reid, and D. McGloin, Opt. Express **14**, 6373-6380 (2006).
[6]W. Y. Chiang, A. Usman, and H. Masuhara, J. Phys. Chem. C **117**, 19182 19188 (2013).
[7]T. C. Preston, B. J. Mason, J. P. Reid, D. Luckhaus, and R. Signorell, J. Opt. **16**, 025702 (2014).
[8]R. M. Power, D. R. Burnham, and J. P. Reid, Appl. Opt. **53**, 8522 8534 (2014).
[9]J. W. Lu, A. M. J. Rickards, J. S. Walker, K. J. Knox, R. E. H. Miles, J. P. Reid, and R. Signorell, Phys. Chem. Chem. Phys. **16**, 9819-9830 (2014).
[10]D. McGloin, Philos. Trans. R. Soc., A **364**, 3521 3537 (2006).
[11]L. Rkiouak, M. J. Tang, J. C. J. Camp, J. McGregor, I. M. Watson, R. A. Cox, M. Kalberer, A. D. Ward, and F. D. Pope, Phys. Chem. Chem. Phys. **16**, 11426 11434 (2014).
[12]J. Bunjarern, L. Mitchem, A. D. Ward, N. H. Nahler, D. McGloin, and J. P. Reid, J. Chem. Phys. **125**, 114506 (2006).
[13]I. Thanopulos, D. Luckhaus, T. C. Preston, and R. Signorell, J. Appl. Phys. **115**, 154304 (2014).
[14]A. E. Carruthers, J. P. Reid, and A. J. Orr Ewing, Opt. Express **18**, 14238 14244 (2010).
[15]J. W. Lu, M. Isenor, E. Chasovskikh, D. Stapfer, and R. Signorell, Rev. Sci. Instrum. **85**, 095107 (2014).
[16]T. Li, S. Kheifets, D. Medellin, and M. G. Raizen, Science **328**, 1673 1675 (2010).
[17]T. Li, *Fundamental Tests of Physics with Optically Trapped Microspheres* (Springer Science and Business Media, 2012).
[18]T. Čižmár, V. Garces Chavez, K. Dholakia, and P. Zemanek, Proc. SPIE **5514**, 643-651 (2004).
[19]A. E. Carruthers, J. S. Walker, A. Casey, A. J. Orr-Ewing, and J. P. Reid, Phys. Chem. Chem. Phys. **14**, 6741 6748 (2012).
[20]C. F. Bohren and D. R. Huffman, *Absorption and Scattering of Light by Small Particles* (Wiley, New York, 1983).
[21]J. D. Eversole, H. B. Lin, A. L. Huston, A. J. Campillo, P. T. Leung, S. Y. Liu, and K. Young, J. Opt. Soc. Am. B **10**, 1955 1968 (1993).
[22]A. A. Zardini, U. K. Krieger, and C. Marcolli, Opt. Express **14**, 6951 6962 (2006).
[23]A. D. Ward, M. Zhang, and O. Hunt, Opt. Express **16**, 16390-16403 (2008).
[24]J. Li, S. T. Wu, S. Brugioni, R. Meucci, and S. Faetti, J. Appl. Phys. **97**, 073501 (2005).
[25]COMSOL Multiphysics®, 2014. Version 4.4. COMSOL, Inc., Burlington, MA, USA, available at www.comsol.com.
[26]M. I. Mishchenko, L. D. Travis, and A. A. Lacis, *Scattering, Absorption, and Emission of Light by Small Particles* (Cambridge University Press, 2002).
[27]M. I. Mishchenko and L. D. Travis, J. Quant. Spectrosc. Radiat. Transfer **60**, 309-324 (1998).
[28]M. I. Cotterell, B. J. Mason, A. E. Carruthers, J. S. Walker, A. J. Orr Ewing, and J. P. Reid, Phys. Chem. Chem. Phys. **16**, 2118 2128 (2014).
[29]A. K. Ray, A. Souyri, E. J. Davis, and T. M. Allen, Appl. Opt. **30**, 3974-3983 (1991).
[30]S. Linkwitz, H. Grabert, E. Turlot, D. Estève, and M. H. Devoret, Phys. Rev. A **45**, R3369 R3372 (1992).
[31]T. X. Phuoc, Opt. Commun. **245**, 27-35 (2005).
[32]V. Shvedov, A. R. Davoyan, C. Hnatovsky, N. Engheta, and W. Krolikowski, Nat. Photonics **8**, 846 850 (2014).